Optimized Model-Free Extremum Seeking Control for Morphing Rotor Systems

Sabine Wisbacher[1] and Daniel Ossmann[1]

***Abstract*— Morphing rotor blades can improve helicopter performance by enabling real-time adaptation of blade shapes for energy-efficient operation. Their highly nonlinear, time-varying aerodynamics and strong coupling between blade configuration and rotor performance make model-based control challenging. This paper presents a model-free, single-input single-output Extremum Seeking Control (ESC) approach for optimizing the steady-state performance of morphing rotor systems. By injecting small perturbations into the morphing input and observing output variations, ESC estimates performance gradients and continuously adapts the blade configuration toward an optimal operating point. The method is computationally efficient, requires no explicit aerodynamic model, and can track optimal performance in real time under uncertainties and varying flight conditions. A novel optimization based approach for finding optimal ESC setting parameters to avoid cumbersome tuning is presented. Simulation results on a Bo 105 simulator demonstrate the effectiveness in achieving energy-efficient rotor operation, highlighting ESC as a practical solution for steady-state operations of morphing rotor systems.**

I. INTRODUCTION

Modern rotor and actuation design of rotorcraft allow for an optimization of vehicle performance Classically, load and power reduction on rotor blades can be realized either using higher harmonic control via the swashplate [1] or via servo actuators replacing the blade pitch links [2]. Modern research strives to adding additional control inputs thus additional degrees of actuation freedoms to enable load and power reductions. A comprehensive study of different mechanisms and their effects is provided in [3], focusing on on-blade active-morphing strategies as active twist and active cambers. It is described in [3], [4] that active cambers perform superior to the use of flaps due to their continuous shape. Thus, in this work such an active chamber on the trailing edge will be explored, which is assumed to be realized via a so-called fishbone mechanism. While in [3] the aerodynamic effects on the steady-state lift and drag behavior of static camber deflections are described, the study is performed purely in open loop, i.e., no active control algorithm is proposed to actually realize the reduced power consumption in steady-state operation.

From a control perspective, rotors with a morphing mechanism represent a challenging control problem due to their highly nonlinear, time-varying aerodynamics and strong coupling between blade shape, thrust, and rotor performance. Traditional model-based optimization or control strategies require accurate aerodynamic models, which are difficult to obtain and maintain for morphing configurations. For high-frequency loads such an approach is generally unavoidable due to the highly coupled dynamics. The energy reduction enabled by the additional degree of freedom by the morphing blades in steady state however, is basically a static optimization problem. Due to model uncertainties, however, the mapping of the blade and morphing angles for different steady-state conditions cannot be precomputed.

Extremum Seeking Control (ESC) is particularly well-suited for this task because it is model-free and can optimize performance directly from measured outputs in real time. By continuously adapting the blade morphing parameters in response to small input perturbations and the observed system response, ESC can track optimal operating points in real time, even in the presence of changing flight conditions or uncertainties. It uses the output variations to estimate the gradient of the performance metric with respect to the input. This gradient estimate is then used to adapt the input toward an extremum, relying on a time-scale separation where the plant settles quickly compared to the slower adaptation. ESC is widely applicable to nonlinear and uncertain systems without requiring an explicit model. [5]

Thus, in this paper an ESC approach is developed for steady-state flight conditions for a helicopter rotor system with active camber morphing capabilities to enabling reductions in the energy consummation. The fast, highly nonlinear dynamics of the morphing rotor system generally call for a computationally cheap algorithm. Thus, the single-input single-output model-free ESC approach, described in detail in Section II, is proposed as solution for finding optimal operation points of the over-actuated system to enable a reduced energy consumption. The ESC's simple, dither-based structure allows for rapid gradient estimation of a performance index and real-time adaptation without requiring a plant model of the rotor nor explicit optimization algorithms. As ESC implements a wide range of free parameters to be selected for an optimal solution, a novel non-linear multi-objective optimization approach to find these parameters is proposed in Section II. A Bo 105 rotor simulation model, detailed in Section III, serves as basis for the verification of the proposed approach. The applicability of the ESC approach to the rotor system depending on its closed-loop system dynamics is discussed in Section IV, providing valuable insight on the ESC design for helicopter rotor systems.

This research was funded by the German Federal Ministry for Economic Affairs and Energy under the grand number 20E2108B entitled *Reglerentwicklung für einen Hubschrauberrotor mit formadaptiven Wölbungsmechanismus* (ARCTIS).

[1]Sabine Wisbacher and Daniel Ossmann are with the Department of Mechanical, Automotive & Aeronautical Engineering, Munich University of Applied Sciences HM, Dachauer Strasse 98b, 80335 Munich, Germany. {sabine.wisbacher, daniel.ossmann}@hm.edu

II. Extremum Seeking Control

Extremum Seeking Control (ESC) is a real-time optimization framework that drives a system toward the minimizer or maximizer of an unknown steady-state map. Unlike gradient-based or model-based controllers, ESC does not rely on explicit knowledge of the plant dynamics. Instead, it uses online perturbation and demodulation to recover gradient information from input-output measurements. This makes ESC well suited for systems where the physics are complex, nonlinear, or uncertain, such as aerodynamic optimization of rotor blades with morphing capabilities.

The standard ESC architectures assembles the periodic input perturbation, a high- and a low-pass filter ([6], [7]) together with the integration and the feedback gain. The core idea is a sinusoidal perturbation and a followed gradient extraction. The authors in [8], [9] have shown, that the original version of the ESC with the tow filters can be implemented without the filters, resembling the very same theoretical behavior. Thus, the too filters are mainly used to increase robustness, i.e., filtering out noise in case of the low pass filter, and removing steady offsets as well as slowly-varying components via the high-pass filter.

A. ESC Fundamentals

Consider a physical system described by its the state vector $x(t) \in \mathbb{R}^n$ and control input $\theta(t) \in \mathbb{R}^{m_u}$. The measured outputs are given by

$$J(t) = \Phi(x(t), \theta(t)), \tag{1}$$

where $\Phi : \mathbb{R}^n \times \mathbb{R}^{m_u} \to \mathbb{R}^{m_y}$ is an unknown, potentially nonlinear function that may vary with operating conditions. It is assumed that $\Phi(\dots)$ satisfies the smoothness conditions required for the application of ESC [5]. Note, while the system itself may have various inputs and outputs as well as additional control loops, for the ESC design only the single-input single-output case is considered in what follows, i.e., $\Phi : \mathbb{R}^n \times \mathbb{R} \to \mathbb{R}$. The constraints on the system dynamics and implications for other available control loops are provided in the discussions below.

The objective of extremum-seeking control (ESC) is to adjust the scalar control $\theta(t)$ online such that the performance function is minimized, i.e.,

$$\theta^\star = \arg\min_{\theta} \Phi(x(t), \theta), \tag{2}$$

or analogously for maximization. A key assumption is that the system states $x(t)$ evolve sufficiently faster than the ESC adaptation, allowing the performance output $J(t) = \Phi(x(t), \theta(t))$ to be considered quasi-steady relative to $\theta(t)$ and enabling the use of classical averaging theory.

ESC relies on injecting a periodic perturbation via the input

$$\theta(t) = \hat{\theta}(t) + a\sin(\omega t) + \theta_0(t), \tag{3}$$

where $a > 0$ is small and ω is large and $\theta_0(t)$ is a considered trim value. Note that the trim value should change more slowly than the ESC adaptation to avoid perturbing the gradient estimation and to preserve time-scale separation. Overall note that this requires the plant dynamics to be faster than the ESC adaptation, and the ESC adaptation to be faster than changes in the trim value.

Because J depends on θ, the oscillation induces a modulation in $J(t)$, i.e.,

$$J(t) = \Phi\big(\hat{\theta}(t) + a\sin(\omega t)\big). \tag{4}$$

A first-order Taylor expansion yields

$$J(t) \approx \Phi(\hat{\theta}) + a\Phi'(\hat{\theta})\sin(\omega t) + \mathscr{O}(a^2) \tag{5}$$

where $\mathscr{O}(a^2)$ represents higher-order terms in the perturbation amplitude a, and $\Phi'(\hat{\theta}) = \frac{d\Phi}{d\theta}\big|_{\theta=\hat{\theta}}$. Note that the dependence on $x(t)$ is suppressed in (4) and (5) due to the quasi-steady assumption, which makes it irrelevant for the gradient computation.

In case a high-pass washout $\mathscr{H}\{\cdot\}$ is used, the measured output is processed first through this filter, i.e.,

$$\tilde{J}(t) = \mathscr{H}\{J(t)\} \tag{6}$$

to remove constant or slowly varying components. Let the high-pass filter $\mathscr{H}\{\cdot\}$ be parameterized by $\mathbf{p}_{\mathscr{H}} \in \mathbb{R}^h$ collecting the parameters of its realizations. In the simplest, i.e., the linear, case, a first order filter with a bandwidth as only parameter can be employed.

Multiplying the filtered output with the perturbation signal results in

$$\tilde{J}(t)\sin(\omega t) \approx \Phi(\hat{\theta})\sin(\omega t) + \frac{a}{2}\Phi'(\hat{\theta})\big(1 - \cos(2\omega t)\big), \tag{7}$$

which contains a constant component proportional to the gradient. A subsequent low-pass filter $\mathscr{L}\{\cdot\}$ removes the oscillatory terms, noise and averages out the constant term, i.e., the gradient estimate

$$\widehat{\Phi'}(\hat{\theta}) \propto \mathscr{L}\{\tilde{J}(t)\sin(\omega t)\}. \tag{8}$$

Let the low-pass filter $\mathscr{L}\{\cdot\}$ be parameterized by $\mathbf{p}_{\mathscr{L}} \in \mathbb{R}^l$ collecting the parameters of its realizations.

By (8), the ESC extracts gradient information $\widehat{\Phi'}(\hat{\theta}) \approx \frac{a}{2}\Phi'(\hat{\theta})$ from (7) first order approximation through persistent excitation and demodulation, without requiring a model of the plant.

Note that the gradient estimate is scaled with the parameter a. Thus, a small perturbation amplitude a results in slow convergence of the gradient estimate, whereas too large values make the first order approximation inaccurate due to the influence of higher-order terms $\mathscr{O}(a^2)$. The low-pass bandwidth ω_c determines how closely the gradient estimate tracks the true constant component.

With the gradient estimate $\widehat{\Phi'}(\hat{\theta})$ available, the adaptation law is defined as

$$\dot{\hat{\theta}} = k\mathscr{L}\{J(t)\sin(\omega t)\}, \tag{9}$$

with $k > 0$ being the adaptation gain. For sufficiently small a and sufficiently high ω, classical averaging theory shows that the closed-loop dynamics behave as

$$\dot{\hat{\theta}} = ka\Phi'(\hat{\theta}) + \mathscr{O}(a^2), \tag{10}$$

which approximates a gradient descent on the unknown map $\Phi(\theta)$. Consequently, $\hat{\theta}(t)$ converges to a neighborhood of the extremum of $\Phi(\theta)$. The size of the neighborhood around the extremum depends on the perturbation amplitude a and the smoothing properties of the low-pass filter, which determine how strongly the oscillatory terms are attenuated. Note that for linear filters this is simply indicated by the filter's bandwidth. Finally, the gradient is integrated via

$$\hat{\theta}(t) = \int_0^t \dot{\hat{\theta}}(\tau)\, d\tau \tag{11}$$

to derive the absolute control signal in (3). ESC is therefore a dynamical system that approximates the solution of an optimization problem through online estimation of the gradient, achieving convergence without any model knowledge. Figure 1 shows a schematic illustration of the dynamic ESC structure.

B. ESC Parameter Tuning

A main task during the setup of ESC is the selection of the different parameters. The free parameters are the adaptation gain k, perturbation amplitude a, perturbation frequency ω as well as the high-pass and low-pass filter coefficients $\mathbf{p}_{\mathscr{H}}$ and $\mathbf{p}_{\mathscr{L}}$, respectively. Setting these parameters can be a cumbersome tasks simply as they influence each other, often leading to a sub-optimal solution in the design. To overcome this issue, a novel approach via non-linear optimization is proposed herein.

All optimization parameters are collected in the vector

$$\mathbf{q} = \left[\mathbf{p}_{\mathscr{H}}^\top, \mathbf{p}_{\mathscr{L}}^\top, a, \omega, k\right]^\top \in \mathscr{Q},$$

where $\mathscr{Q}$ denotes the feasible set. A multi-objective min-max optimization problem is then formulated as

$$\begin{aligned} \min_{\mathbf{q}\in\mathscr{Q}} \quad & \max_i w_i^{-1} c_i\big(x(t),\theta(t);\mathbf{q}\big), && i = 1,\dots,n_c, \\ \text{s.t.} \quad & \tilde{w}_j^{-1} h_j\big(x(t),\theta(t);\mathbf{q}\big) \leq 0, && j = 1,\dots,n_h, \\ & \mathbf{q}_{\min} \leq \mathbf{q} \leq \mathbf{q}_{\max}, \end{aligned} \tag{12}$$

subject to $x(t)$ and $\theta(t)$ being generated by the simulation model with the specified parameters, and $c_i(\cdot)$ denoting the i-th performance optimization metric. Additionally, via $h_i(\cdot)$ hard optimization constrains can be included in the optimization problem, likewise upper and lower bounds on the optimization parameters, i.e. $q_{\min}$ and $q_{\max}$, respectively. The weightings w_i and $\tilde{w}_j$ are used to scale the optimization criteria and the optimization constraints properly. For solving the optimization problem (12) standard nonlinear optimization tools can be used, e.g., the ones provided in Matlab's Optimization Toolbox.

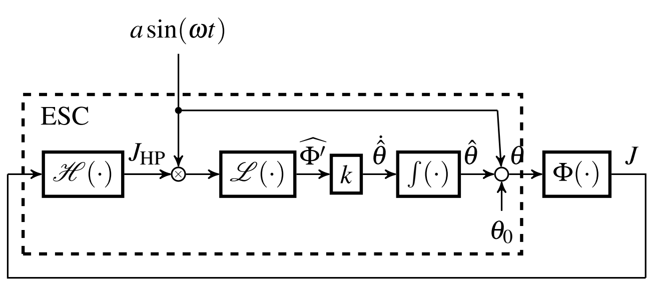

Fig. 1. Schematic illustration of the dynamic ESC structure.

III. Morphing Rotor Modeling

The model of the underlying rotor for the ESC study includes the blade itself as well as the active chamber section on this blade. Generally, high fidelity rotor models involve structural dynamics and aerodynamics and are computationally expensive to run. This makes them somewhat unsuitable for an initial simulation based controller design as controller design iterations may last for hours. The control problem herein is defined by finding an appropriate morphing angle which enables a reduced drag reduction thereby describe the overall required torque τ provided by the helicopter's engine. While drag D is to be reduced the total lift L needs to stay constant via the blade pitch setting to maintain the current steady state state of the helicopter. A graphical illustration of a rotor blade with an active chamber and the main acting forces is depicted in Fig. 2.

As lift and drag are the main effects to be controlled, a simplified model mainly considering the steady-state aerodynamic characteristics of the blade as well as the actuator dynamics is derived herein. The latter are needed for suitable selection and testing of the ESC periodic control inputs. That said, any structural dynamics of the blades and unsteady aerodynamic effects are neglected in the model used herein. Imposed constraints by the structural dynamics on the ESC design will be, however, explicitly considered in the parameter selection of the ESC. Such a simplification is considered acceptable as the paper introduces a proof of concept of the ESC for rotor performance optimization.

A. Bo 105 Rotor Model

As baseline rotor for the proposed ESC approach herein a simplified model of an isolated Bo 105 hingeless main rotor enhanced with a active chamber model is used, see [3]. The blade aerodynamics are available and have been computed using lifting-line theory based on 2D airfoil characteristics of the NACA23012 at discrete radial stations. The required airfoil polars for the baseline NACA23012 and for the camber morphed airfoil shapes have been provided via [10] using CFD simulations. The aforementioned model has originally been validated using data available in literature from test campaigns carried out at the NASA Ames Research Center's 40-by-80-foot wind tunnel using the full-scale Bo 105 rotor [11]. Adequate correlations in rotor trim angles, rotor power,

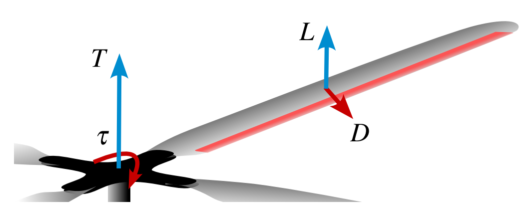

Fig. 2. Graphical illustration of a rotor blade with an active chamber section.

lift-to-drag, and pitch-link loads between the model used herein and the model derived in [11] are given in [12]. For this Bo 105 rotor the original wind tunnel test involved feedforward injection of higher-order individual blade pitch commands. Besides the modeling [12] also proposed open loop techniques for power reduction and loads, while [13] introduces an adaptive control algorithm for the reduction of vibrations on the blades. Overall, with this historic scientific background of the Bo 105 rotor mode, it provides a perfect baseline to test the proposed ESC strategy herein.

The core of the rotor model are the aerodynamic coefficients. The lift coefficient c_L of the model over the rotor blade's angle of attack α is depicted in Fig. 3. The 17 different lines correspond to different morphing deflection angles δ between -9° (—) 13.5° (—) including the neutral morphing angle of 0° (—). Note that in hover flight, the inflow angle of the air to the rotor equals zero degrees. Thus, the rotor's blade pitch angle β equals the angle of the attack α. The polar curves in Fig. 3 show the classical linear shape over the main part of the operating regime, while at high angles of attack the blade starts to stall and lift decreases. The active camber, if defected downwards (positively), increases the effective camber of the blade so that more lift is generated at the same angle of attack. It leads, however, to an earlier stall compared to the neutral morphing angle. If deflected upwards (negatively), the effective camber is reduced reversing the aforementioned effects. In Fig. 4 the corresponding drag coefficient c_D over the angle of attack α for the 17 different morphing angles is depicted. It shows the typical quadratic-like shape over the relevant angle of attack regime. For a constant angle of attack and a downward deflection, the lift increases and so does the induced drag.

The considered hover condition of the rotor demands an angle of attack of about 8° [12], giving a lift coefficient c_L of 1.078 (○). As the lift of the rotor needs to be maintained in steady state operations, an ESC can effectively search along the horizontal line of constant c_L shown in Fig. 3 via (- - -). Respecting the minimum and maximum available morphing angles, this gives a possible angle of attack range from about 0.3° to about 15°. The trim angle of attack value of 8° gives a drag coefficient c_D of $1.47 \cdot 10^{-2}$ as indicated in Fig. 4 via (○). The goal is to reduce the drag by changing the

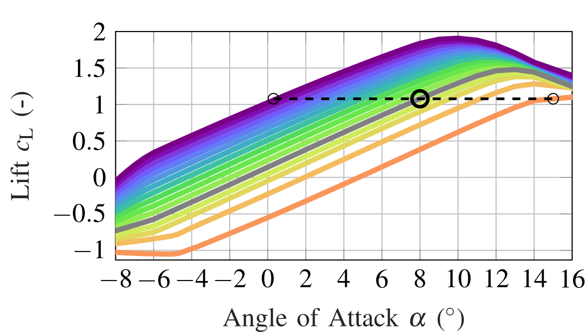

Fig. 3. Lift coefficient for different morphing deflection.

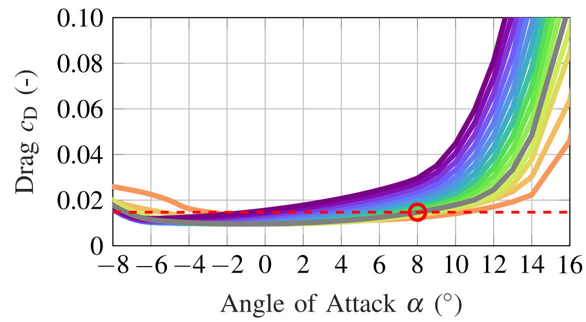

Fig. 4. Drag coefficient for different morphing deflection.

angle of attack, reaching any point below the straight line (- - -) in Fig. 4, while maintaining a c_L of 1.078. This leaves the ESC mainly with the option of reducing the angle of attack. While drag can also be reduced by increasing the angle of attack, the potential for drag reduction is higher when reducing the angle of attack. With these initial findings available it is reasonable to aim for an ESC design and enable the potential of the active camber with respect to a reduction of the energy consumption.

IV. ESC for Morphing Rotors

The ESC for the Bo 105 helicopter rotor aims to reduce the power consumption in steady-state flight conditions while maintaining lift. With active cambers on each blade the rotor is an over-actuated system which can be used to solve this additional task. While constant lift is required to maintain the steady-state flight condition, lower power consumption is realized via lower drag generated from the airfoils. Drag, directly proportional to the driving moment, is assumed to be measurable directly at the drive train, e.g., via stain gauges on the main shaft of the drive train. Lift on the other hand can usually not be directly measured, but steady-state estimates are provided via the current helicopter conditions. Herein, it is assumed that lift and drag are available and can be used in the control algorithm. The proposed control system features a proportional-integral controller to maintain thrust via the blade pitch β, which directly changes the blades' angles of attack via the blade pitch. The ESC is changing the morphing angle δ on each blade to reduce the drag. The ESC excitation is applied identically to all blades, resulting in a purely collective morphing input. A block diagram of the proposed control system is depicted in Fig. 5.

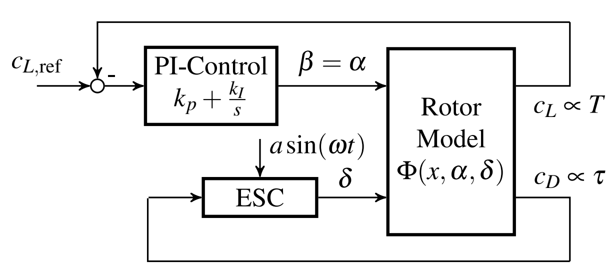

Fig. 5. Proposed morphing rotor controller architecture.

A. ESC Setup

As introduced in Section II, the plant dynamics need to be faster than the ESC adaptation, and the ESC adaptation to be faster than changes in the trim value. As the ESC targets steady state loading on the helicopter, trim changes of the pilot are considered. Referring to [14], piloting tasks associated with the flight-path geometry, i.e., guidance, are limited to a bandwidth below 0.3 Hz. See also [15], [16] for further discussions on the associated frequencies with helicopter handling qualities and workload. On the other end, the Bo 105 has a once per revolution frequency of $\phi = 7\,\text{Hz}$. Due to the fact that for maneuvering once per revolution commands need to be issued via the swashplate, typical actuation systems require a bandwidth above 10 Hz. The first structural modes $\omega_i^{(s)}$ with $i = \{1,2,3\}$ of the blades are located at 2.5 Hz, 3.2 Hz and 9.7 Hz. These mode are valid, however, in the rotating frame of the rotor, while the ESC operates on the fixed frame, simply as shaft torque is measured in the fixed frame. Mapping these three frequencies in the non-rotating frame using the rotation frequency of 7 Hz and $|\phi - \omega_i^{(s)}|$ to compute the lower mapping of the transformed frequencies gives 4.5 Hz, 3.8 Hz and 2.7 Hz, respectively [17]. Note that the other, i.e., higher frequency, mapping are not of interest because they result in higher frequencies. Likewise holds for any other structural models of higher frequency. The limiting upper frequency thus is 2.7 Hz. Considering the bounds of 0.3 Hz and 2.7 Hz together with a factor of 2, the ESC excitation frequency needs to be selected from the tight frequency band of 0.6 Hz and 1.25 Hz to ensure the required time scale separation. Note that while actuators, structural dynamics and pilot excitation is accounted for here, structural coupling of the rotor and the helicopter cell and possible inflow excitations are not. In case these effects lie in the range of the ESC excitation a different selection of the excitation frequency or additional filtering may become necessary.

Based on these discussion, the ESC parameters are initialized as follows: an excitation frequency of $\omega = 0.9\,\text{Hz}$, a first-order low-pass filter with cutoff $\omega_{\mathscr{L}} = (2\pi)^{-1}\,\text{Hz}$, a first-order high-pass filter with cutoff $\omega_{\mathscr{H}} = (2\pi)^{-1}\,\text{Hz}$, and an adaptation gain of $k = 10$. The amplitude of the sine wave is fixed to a value of 0.1°, which provides a large enough excitation for the gradient extraction without generating too large lift fluctuations. The simulation time is fixed to 30 s, as within this time window, the ESC is supposed to settle. This initial guess for the ESC parameters already provides a reduction of 3.5% of required energy. A closer look toward the blade pitch commands and morphing inputs, however, reveals that the input signals have not fully settled within the 30 s. For example the blade pitch angle still shows a changing rate of 0.13°/s, which is considered to be non-adequate as a faster transition to steady-state is required.

B. Optimization-based Parameter Tuning

As the manual tuning of the parameters becomes cumbersome, the nonlinear optimization setup following (12) is defined to improve the results. As tuning parameters the corner frequencies of the first order filters, the frequency of the excitations and the adaptation gain are selected, i.e.,

$$\mathbf{q} = \left[\omega_{\mathscr{H}}, \omega_{\mathscr{L}}, \omega, k\right]^\top.$$

Note that compared to (12) the excitation amplitude a is not included as it is chosen by physical reasoning as described before. For the upper and lower limits of the filters values of $0.1(2\pi)^{-1}$ Hz and 0.6 Hz are selected, respectively. While the lower bound ensures that the filter frequencies are not getting too small, the upper bound ensures that the frequencies of the filters stay below the lower bound of the perturbation frequency ω, which has been defined at 0.6 Hz in the last section. Finally, the adaptation gain k shall maintain between values of 5 and 15, ensuring an adequately fast but not overly aggressive adaptation.

As optimization criterion in (12) the drag at the end of the simulation T is selected, i.e., $c_1 = c_D(T)$. A weight of $w_1 = 100$ is selected to bring the criterion towards a value of 1, which improves optimization performance. To explicitly account for the requirement that the ESC has been achieved steady state operation after the 30 s, the derivative $\dot{\beta}(T)$ of the blade pitch angle is used to define the optimization constraint $h_1 = \dot{\beta}(T) - 10^{-3}$ with $\tilde{w}_1 = 1$ is defined. This effectively demands a blade pitch motion of less than 0.001°/s at the end T of the simulation. The optimization using Matlab's `fmincon` constraint optimization function is completed in approximately 100 s on a standard laptop with an Intel Core i7-1365U processor and 32 GB RAM. The resulting optimized parameters are listed in Table 1 together with the initialized values and the selected parameter bounds. Finally, a reduction of 4.8% of required energy is achieved, increasing the improvement by 1.3% compared to the initialized values. Note that mainly the filter parameters are changed by the optimization, while the adaptation gain and perturbation frequency have been initialized well via the physical-based interpretation.

TABLE I
INITIALIZED AND OPTIMIZED ESC PARAMETERS.

	$\omega_{\mathscr{L}}$ (Hz)	$\omega_{\mathscr{H}}$ (Hz)	ω (Hz)	k (-)
initialized	0.16	0.16	0.90	10
optimized	0.09	0.07	0.90	9.95
bounds	[0.016,0.6]	[0.016,0.6]	[0.6,1.25]	[5,15]

C. Simulation Results

Figure 6 shows the blade pitch angle and thus the angle of attack in the upper diagram and the morphing angle in the lower diagram over the 30 simulation time. Starting at the trim values ( ) of 8° in blade pitch and 0° in morphing angle, the ESC is activated at the beginning of the simulation. For the initially chosen values ( ) the blade pitch converges to 6.2° while the morphing angle settles at 2.6°. Again, the blade pitch angle in this scenario still shows an averaged gradient of 0.13°/s. With the optimized parameters ( ) blades pitch as well as morphing angles

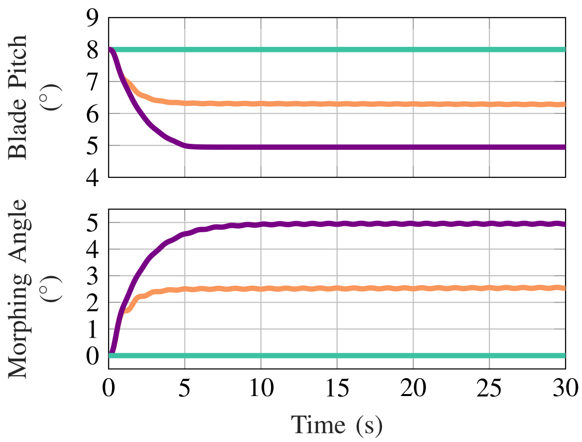

Fig. 6. Rotor inputs with ESC scheme in hover.

settle around 5° with effectively zero averaged gradient thanks to the considered optimization constraint.

Figure 7 uses the same color coding as Fig. 6 and depicts the lift value in the upper and the drag in the lower diagram. While trim-lift is restored in both cases adequately fast by the same proportional-integral controller within 5 s, drag reduction is increased by 1.3 % by the optimized parameter set. Overall the optimized parameter set takes a bit more time simply because the change in the inputs lasts longer, see Fig 6. Finally, Fig. 8 depicts a zoomed-in version of the drag coefficient from Fig. 4 showing at which value and blade pitch, i.e., angle of attack, starts (○) and settles after the optimization (○), indicating how delicate the optimization process in terms finding the drag minimum is. Overall the found reduction of 4.8% confirms the findings in [3], but achieves them within an actual closed control loop.

V. Conclusion

An extremum seeking control strategy is implemented for a helicopter rotor to enable required power reduction. A novel optimization- and simulation-based design method is proposed to map the ESC setting parameters to intuitive tuning criteria. The proposed approach is successfully applied to a simplified Bo 105 rotor simulation model, achieving the desired power reduction in steady state operating conditions.

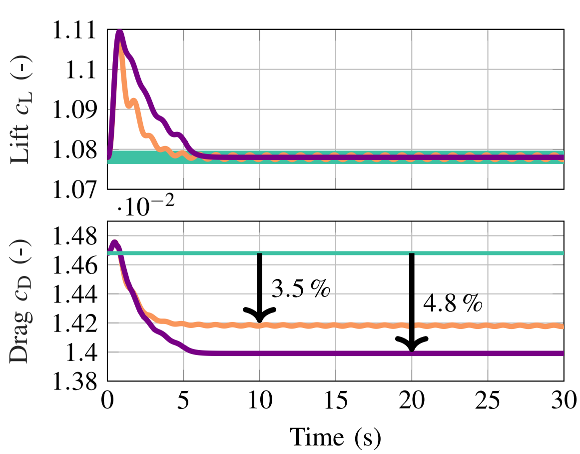

Fig. 7. Rotor outputs with ESC scheme in hover.

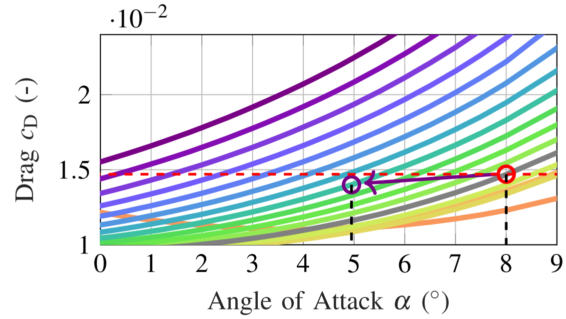

Fig. 8. Drag coefficient at with (○) and without ESC (○).

References

[1] K. Nguyen and I. Chopra, "Application of higher harmonic control to rotors operating at high speed and thrust," *Journal of the American Helicopter Society*, vol. 35, no. 3, pp. 78–89, 1990.

[2] S. A. Jacklin, A. Blass, S. M. Swanson, and D. Teves, "Second test of a helicopter individual blade control system in the nasa ames 40-by 80-foot wind tunnel," in *American Helicopter Society 2nd International Aeromechanics Specialists' Conference*, Bridgeport, CT, USA, 1995.

[3] J. Rauleder, B. G. van der Wall, A. Abdelmoula, D. Komp, S. Kumar, V. Ondra, B. Titurus, and B. K. S. Woods, "Aerodynamic performance of morphing blades and rotor systems," in *74th Annual American Helicopter Society International Forum*, Phoenix, AZ, USA, 2018.

[4] R. Jain, H. Yeo, and I. Chopra, "Investigation of trailing-edge flap gap effects on rotor performance using high-fidelity analysis," *AIAA Journal of Aircraft*, vol. 50, no. 1, pp. 140–151, 2013.

[5] D. Dochain, M. Perrier, and M. Guay, "Extremum seeking control and its application to process and reaction systems: A survey," *Mathematics & Computers in Simulation*, vol. 82, no. 3, pp. 369–380, 2011.

[6] M. Guay and D. Dochain, "A proportional-integral extremum-seeking controller design technique," *Automatica*, vol. 77, pp. 61–67, 2017.

[7] ——, "A time-varying extremum-seeking control approach for discrete-time systems," in *19th World Congress of the International Federation of Automatic Control*, Cape Town, South Africa, 2014.

[8] Y. Tan, D. Nešić, and I. Mareels, "On non-local stability properties of extremum seeking control," *Automatica*, vol. 42, no. 6, pp. 889–903, 2006.

[9] K. B. Ariyur and M. Krstić, *Real-Time Optimization by Extremum Seeking Control*. New York, NY, USA: John Wiley & Sons, 2003.

[10] A. Abdelmoula and J. Rauleder, "Aerodynamic performance of morphed camber rotor airfoils," in *AIAA Scitech Forum*, San Diego, CA, USA, 2019.

[11] R. L. Peterson, "Full-scale hingeless rotor performance and loads," NASA Ames Research Center, Technical Memorandum NASA-TM-110356, 1995.

[12] D. Komp, S. Kumar, M. Hajek, and J. Rauleder, "Effect of active camber morphing on rotor performance and control loads," *Aerospace Science and Technology*, vol. 108, p. 106311, 2021.

[13] S. Kumar, D. Komp, M. Hajek, and J. Rauleder, "Integrated rotor performance improvement and vibration reduction using active camber morphing," in *ASME Conference on Smart Materials, Adaptive Structures and Intelligent Systems*, Louisville, KY, USA, 2019.

[14] W. Memon, M. D. White, G. D. Padfield, N. Cameron, and L. Lu, "Helicopter Handling Qualities: A study in pilot control compensation," *The Aeronautical Journal*, vol. 126, no. 1295, pp. 152–186, 2022.

[15] G. Padfield, M. Charlton, J. Jones, S. Howell, and R. Bradley, "Where Does the Workload Go when Pilots Attack Manoeuvres?: An Analysis of Results from Flying Qualities, Theory and Experiment," in *20th European Rotorcraft Forum*, Amsterdam, The Nederlands, 1994.

[16] J. Jones, G. Padfield, and M. Charlton, "Wavelet analysis of pilot workload in helicopter low-level flying tasks," *The Aeronautical Journal*, vol. 103, no. 1019, pp. 55–63, 1999.

[17] R. Coleman and A. Feingold, "Theory of self-excited mechanical oscillations of helicopter rotors with hinged blades," Langley Aeronautical Laboratory, Tech. Rep. Technical Note 3844, 1958.